Cohesive simulation of hydrogen assisted crack initiation in X70 steel and welded joints

*Vigdis Olden, SINTEF, 7054 Trondheim, Norway (vigdis.olden@sintef.no),
www.sintef.no, Odd Magne Akselsen, SINTEF and NTNU, Norway
(odd.m.akselsen@sintef.no), Hallvard Fjær, IFE, 2027 Kjeller, Norway
(hallvard.fjar@ife.no), www.ife.no*

Summary

Fracture mechanics SENT testing and FE modelling to establish hydrogen influenced cohesive parameters for X70 structural steel have been performed. Base metal and weld simulated coarse grained heat affected zone have been included in the study. An example of application of the cohesive model in structural integrity assessments of welded joints have also been carried out. Base metal X70 did not fail at net section stresses lower than 1.29 times the yield strength and revealed low sensitivity to hydrogen embrittlement. Weld simulated coarse grained heat affected zone was prone to fracture at stresses above 70% of the yield strength, which indicates hydrogen embrittlement susceptibility. Cohesive parameters were δ_c=0.3 mm and σ_c=1700 MPa (3.5·σ_y) for base metal and δ_c=0.3 mm and σ_c=3900 MPa (4.8·σ_y) for coarse grained heat affected zone.

Introduction

Weld repair at deep waters, so called hyperbaric welding, introduces several challenges. Dry hyperbaric gas tungsten arc (GTA) or gas metal arc (GMA) welding is performed in a pressure chamber. Due to arc constrictions imposed by the pressure, smaller weld beads are deposited than in conventional welding. Accordingly, the associated cooling rates, expressed at the cooling time between 800 and 500 degrees C (Δ $t_{8/5}$), will be faster, which in turn, may give higher weld metal and heat affected zone hardness. Moreover, in hyperbaric tie-ins or hot tapping, certain welds may be deposited under high restraint conditions. Thus, in the presence of moisture in the welding atmosphere (chamber gas, shielding gas, contaminants in the groove), the combination of rapid cooling and high restraint intensity may introduce cold cracking (hydrogen embrittlement) problems. Due to the narrower operational window under hyperbaric conditions, the welding parameter selection and preheating are constrained. Therefore, modelling and simulation of the welding process and subsequent pipe integrity will be very useful to reduce the extent of welding and testing trials.

In recent years the cohesive zone modelling (CZM) approach has gained interest in finite element modelling (FEM) of hydrogen induced fracture. The method is appealing due to the possibility of modelling the fracture without taking the detailed micro-mechanism into account; it simply addresses the reduced energy threshold due to the presence of hydrogen. Fracture takes place at an interface of cohesive zone elements embedded in a finite element model; no continuum elements are damaged in a cohesive model. The cohesive elements can be pictured as two faces separated by a thickness, which is close to zero. The relative motion of the top and bottom faces in the thickness direction represents opening or closing of the interface. The relevant constitutive "material" response is a traction-separation description; an evaluation which gives the amount of energy required to create new surfaces. A

traction separation law (TSL) is a function described by the cohesive stress, σ(δ), and separation, δ. The area below the curve represents the critical separation energy, Γ$_c$.
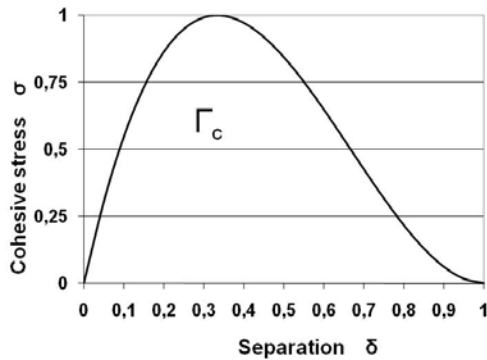
Figure 1 Polynomial traction separation law, TSL

This paper will present a FE method of simulating hydrogen crack initiation using hydrogen influenced cohesive elements. The model, including the governing equations for hydrogen diffusion and cohesive modelling will be presented in the first paragraph. The results section includes a presentation of the fracture mechanics experimental testing of X70 structural steel in the as received (base metal) and in weld simulated coarse grained heat affected zone (CGHAZ) condition. Furthermore results from FE simulations will be described and compared to the experiments. The result section also includes an example of application of the model on a simplified welded joint geometry in X70 structural steel. Finally, the results are discussed, some major conclusions drawn and further work proposed.

The model
The applied model consists of a three step FE simulation procedure including elastic-plastic stress analysis, diffusion analysis and finally elastic-plastic stress analysis with hydrogen influenced cohesive elements implemented in the crack path. The applied FE code was ABAQUS Standard version 6.5 and 6.9[1].

Elastic plastic stress analysis
The elastic plastic stress analysis is performed using the standard Mises material model in ABAQUS Standard with a material specific stress-strain curve for the base metal (BM) and the weld simulated CGHAZ. The resulting stress field at each applied stress level is given as an initial condition to the diffusion analysis.

Diffusion model
Stress driven diffusion given in ABAQUS is represented by a modified Ficks' law with respect to the hydrostatic stress, p:

$$\frac{\partial C}{\partial t} = D\nabla^2 C + D \cdot \frac{V_H}{R \cdot \left(T - T^Z\right)} \nabla C \cdot \nabla p + D \cdot \frac{V_H}{R \cdot \left(T - T^Z\right)} C\nabla^2 p \qquad (1)$$

Where C is the hydrogen concentration, D is the diffusion coefficient, V_H is the partial molar volume of hydrogen in iron-based alloys, R the gas constant (8.3142 J/mol K), T the actual and the absolute zero temperature, see ABAQUS manuals or earlier work[2] for details.

The treatment of crack tip hydrogen concentration has traditionally been based on Eq. 1 representing an accumulation of hydrogen in areas of high hydrostatic stress. Sofronis and McMeeking[3] and later Krom and Bakker[4] described diffusion models reflecting a competition between the hydrostatic stress field and the highly strained area at the notch tip. The models are based on the principle by Oriani[5] that populations of hydrogen in trapping sites and in lattice always are in equilibrium, as described by:

$$\frac{\theta_T}{1-\theta_T} = \frac{\theta_L}{1-\theta_L} K_T \tag{2}$$

θ_L denotes the occupancy of hydrogen on interstitial lattice sites, θ_T the occupancy of hydrogen on trapping sites and $K_T = e^{\frac{-E_T}{RT}}$. Details of the model can be found in refs 2-4.

In the present work a simplified approach based on the work by Taha & Sofronis[6] is proposed. FE calculations for high and low strength steel revealed that the shape of the plastic strain distribution and of the hydrogen concentration in traps in front of a crack tip when exposed to surface hydrogen were almost similar, *Figure 2*. A marginal influence of the strain rate due to the easy access of hydrogen from the surface was observed. Based on the reported data in[6] we propose a linear correlation between the trapped hydrogen concentration and the plastic strain:

$$C_T = (49.0 \cdot \varepsilon_p + 0.1) \cdot C_L \tag{3}$$

The relation implies that when the plastic strain is larger than ~ 2%, trapping will yield the dominating influence on the hydrogen concentration. The correlation is implemented in a user defined cohesive element subroutine. By reading the plastic strain in the neighbouring continuum elements C_T is calculated and added to C_L for each increment and node before giving the total hydrogen concentration C to the TSL. The coupling between hydrogen diffusion and cohesive zone modelling can be unidirectional, i.e. the hydrogen concentration affects the cracking behaviour but not vice versa, or bidirectional (fully coupled). The latter provokes the mechanical field quantities (stresses and strains) to affect the hydrogen diffusion as well. In the present paper the modelling is unidirectional. The hydrogen distribution history as a function of a constant stress field is implemented into cohesive elements. The cohesive element includes a subroutine taking hydrogen concentration from plastic strain (trapping) into account.
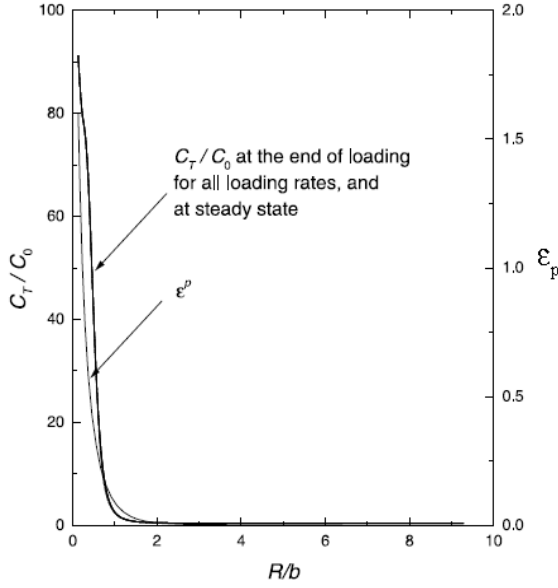
Figure 2 Normalized hydrogen concentration (C_T/C_0)in trapping sites and equivalent plastic strain as a function of the normalized distance (R/b) from a blunted crack tip in steel as reported by Taha & Sofronis[6].

Cohesive model
Perhaps the most frequently used TSL is the polynomial function proposed for fracture in ductile materials first introduced by Needleman[7] and further developed by Tvergaard[8]. This is also the shape of the TSL applied in the present work:

$$\sigma(\delta) = \frac{27}{4}\sigma_c \frac{\delta}{\delta_c}\left(1 - \frac{\delta}{\delta_c}\right)^2 \ for \, \delta \langle \, \delta_c, \ otherwise \ 0 \tag{4}$$

σ_c denotes the critical cohesive stress, δ_c the critical opening of the cohesive element. The separation energy for the polynomial description is calculated from:

$$\Gamma_c = \frac{9}{16}\sigma_c \delta_c \tag{5}$$

From the separation energy the stress intensity factor K_I can be calculated:

$$K_I = \left[\frac{E \cdot \Gamma_c}{1 - v^2}\right]^{1/2} \tag{6}$$

E is the Young's modulus and v is Poisson's rate.

Note that the present work considers the mode I plain strain opening case and that the influence of variations in stress triaxiality around the crack tip is not evaluated.

4

Hydrogen influenced traction separation law

A relation for the coupling between hydrogen coverage, θ, and the local critical hydrogen dependent cohesive stress, σ_c (θ) for bcc Fe proposed by Serebrinsky et al.[9] is applied:

$$\frac{\sigma_c(\theta)}{\sigma_c(0)} = 1 - 1.0467\theta + 0.1687\theta^2 \tag{7}$$

where $\sigma_c(0)$ is the local critical cohesive stress without hydrogen influence. The relation is based on a fitting of surface energy values reported by Jiang and Carter[10], where the surface energy for α-Fe without hydrogen influence, γ (0), is 2.43 J/m². Hydrogen coverage is defined as a function of the hydrogen concentration and the Gibbs free energy difference of the interface and the surrounding material as expressed in the Langmuir-McLean isotherm[11]:

$$\theta = \frac{C}{C + \exp(-\Delta g_b^0 / RT)} \tag{8}$$

Figure 3 illustrates how the cohesive energy decreases with increasing hydrogen coverage.
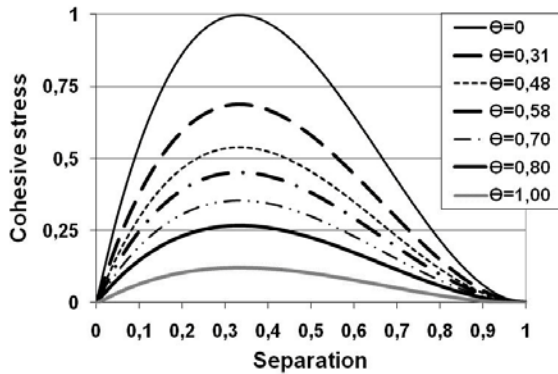
Figure 3 Normalized hydrogen influenced TSL showing decreasing cohesive energy with increasing hydrogen coverage.

Two dimensional user defined cohesive elements are implemented in ABAQUS Standard (6.5 and 6.9) using a FORTRAN sub-routine initially developed by Scheider[12] and further developed by Olden et. al[13].

To add the strain influence on the hydrogen concentration the effective plastic strain in the nearest element to the cohesive elements need to be found and the information transferred to the cohesive elements. To find the strain in certain points the user subroutine UVARM in ABAQUS is used to gather the effective plastic strain for elements where the material definition includes specification of user-defined output variables. An array containing the coordinates and the effective plastic strain for the integration point is created and communicated to the cohesive elements. The

effective plastic strain in the nearest integration points to the surrounding element is transferred to the cohesive element. An extra term in the hydrogen concentration is defined as the hydrogen concentration calculated from the diffusion analysis and the addition to the hydrogen concentration due to plasticity. In the cohesive stress analysis the hydrogen concentration must be given for the nodes connected to the cohesive elements as part of the input to the finite element analysis. Based on the hydrogen concentration for the four nodes connected to an element a mean concentration for the cohesive element can be calculated as

$$C_E = \frac{1}{4}\sum_{i=1}^{4} C_{Ni} \tag{9}$$

The hydrogen coverage in the element is then calculated by Eq. 8 (C is replaced with C_E) and the critical cohesive stress in pure tension for the element is calculated by Eq. 7. Based on the normal separation δ_N in the cohesive element, which is the difference of the displacement of the adjacent continuum elements, a normal stress in the cohesive element is calculated by Eq. 4. When the normal separation δ_N has reached the value of δ_c, the element looses the ability to carry load in both the normal and the transverse direction. In the current work the stresses in the normal and transverse direction for the cohesive element are calculated independent of each other. The shear traction is calculated from the tangential separation and given as a linear law:

$$\sigma_T = \sigma_M \frac{\delta_T}{\delta_M} \tag{10}$$

δ_T is the transverse separation, σ_M and δ_M are input parameters for the actual TSL. The shear traction is independent of the hydrogen concentration and in the current work no unloading in the shear direction of the cohesive element are implemented.

Crack initiation is defined as zero cohesive stress and critical opening (δ_c) in the first cohesive element.

Experiments

Material
Two X70 materials were applied for experimental SENT testing. For base material (BM) testing samples were taken from the longitudinal direction of a pipe with wall thickness 23.3 mm. For testing of the CGHAZ properties, samples were machined from a 40 mm thick X70 hot rolled plate for pipeline production and then weld simulated. Chemical compositions of the two steels are given in Table 1.

Yield ($R_{p0.2}$) and ultimate tensile strength for the BM are 485 MPa and 600 MPa. Weld simulated CGHAZ tensile properties are $R_{p\ 0.2}$ =809 MPa and R_m=1050 MPa. Prior to specimen notch preparation, weld simulation was performed. CGHAZ properties were obtained by heating up to a peak temperature of about 1350°C followed by direct quenching in water. Representative micrographs of the BM and weld simulated CGHAZ microstructure in the longitudinal direction are given in *Figure*

4. Microstructure of the pipe material is ferritic-pearlitic, *Figure 4*a, while weld simulated GCHAZ is bainitic-martensitic, *Figure 4*b.

Table 1 Chemical composition of X70 steels applied for SENT testing (weight %)

	C	Mn	Si	P	S	Cu	Mo	Ni	Cr	Ti	P_{cm}
X70 (CGHAZ)	0.047	1.74	0.10	0.01	7 ppm	0.32	0.04	0.25	0.05	0.01	0.16
X70 (BM)	0.09	1.71	0.30	0.01	10 ppm		0.02	0.05	0.07	0.02	0.20

SENT testing

Fracture mechanics single edge notch tension (SENT) specimens were used for testing of constant load hydrogen influenced fracture resistance. The geometry is given in *Figure 5*. For BM specimens a fatigued notch of 2 mm was applied. To avoid deformation outside the weld simulated notch area of the CGHAZ specimens, the fatigued notch was increased to 6 mm. Prior to testing, the samples were electrolytically hydrogen charged in 3% NaCl at 80°C at a potential of -1050 mV$_{sce}$ for a week to a hydrogen concentration of maximum 1.5 ppm (measured by melt extraction). To avoid hydrogen escape the samples were kept at cathodic potential (CP) of -1050 mV$_{sce}$ also during testing, but at a temperature of 4°C representing subsea operating conditions. *Figure 6* shows a picture of the test set up.
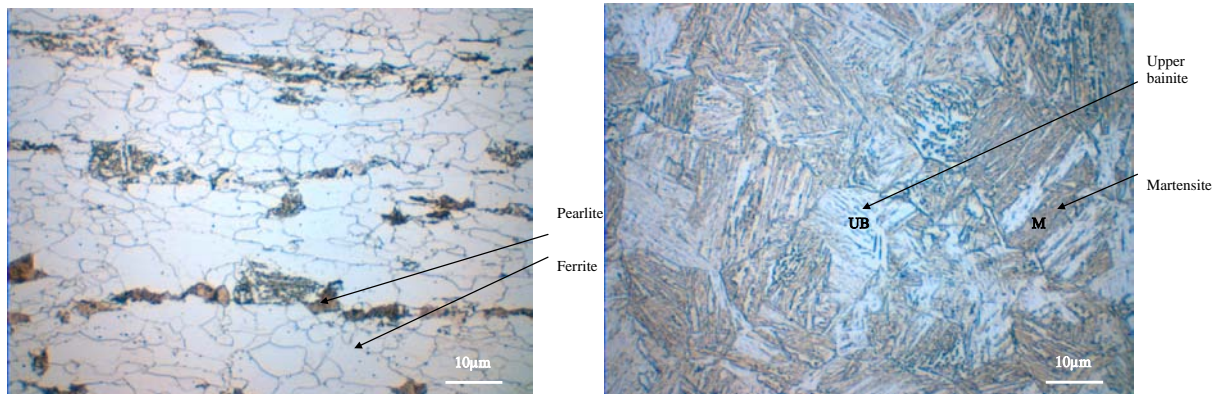
Figure 4 Microstructure of X70 steel a) Base metal b) Weld simulated CGHAZ
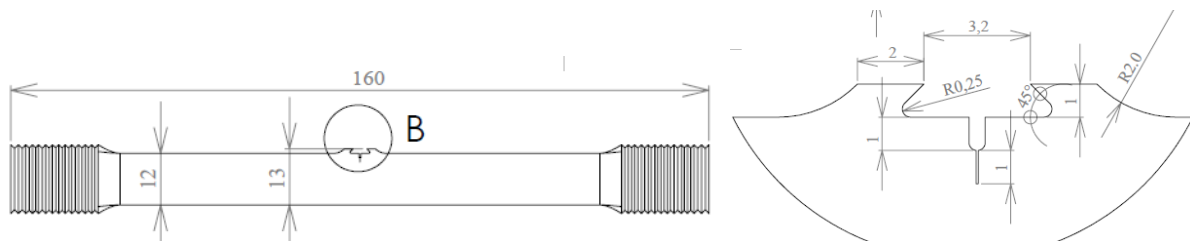
Figure 5 SENT specimen geometry including detail of the notch area with grips for extensometer.

Figure 6 Test set up for the constant load SENT testing at CP conditions.

To establish the required cohesive energy (Γ_c) prior to ductile crack growth, J-r fracture mechanics testing of uncharged specimens were performed in air at 4°C. This identifies the initial values of cohesive stress $\sigma_{c(0)}$ and cohesive opening δ_c in the FE simulations (ref eq 5, 6 and 7). By measuring the length of the deformed area prior to crack growth in optical microscope after testing, a mean stretching zone width (SZW) of 0.1 mm was found for the base metal specimens. This represents an energy of about 300 N/mm, see Figure 7a. The SZW was not easy to identify in the CGHAZ specimen. An assumed SCZ of 0.1 mm also in these specimens, gives an energy of 400 N/mm, see Figure 7b. These J values works as an approximation of the initial cohesive energy.

a)   b)
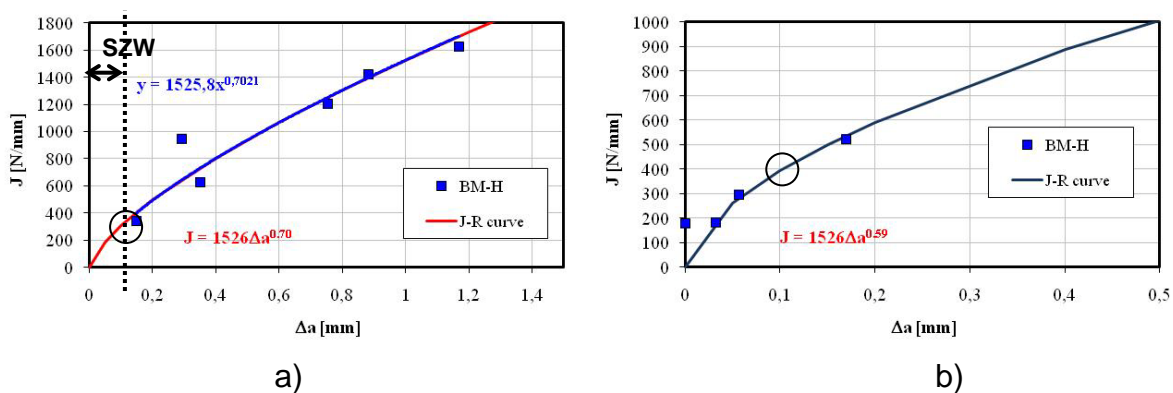
Figure 7 J-r curves from SENT-testing of uncharged specimens. A stretching zone width (SZW) of 0.1mm represents an energy of about 300 N/mm in the BM specimens (a) and 400 N/mm in the CGHAZ specimens (b), which gives an estimation of the initial cohesive energy prior to hydrogen influence.

Constant load SENT testing was performed in the net section stress range 580 – 640 MPa for BM and 650 – 880 MPa for the CGHAZ specimens. Plots showing initial crack mouth opening displacement (CMOD) and net section stress as a function of time to fracture are presented in *Figure 8*. For the BM specimens fracture did not occur below a net section stress of 620 MPa wich is close to the ultimate tensile stress without hydrogen, see *Figure 8*a. This is an indication of low sensitivity to hydrogen. In the CGHAZ specimens fracture occurred at net section stresses well below the yield stress, indicating a clear influence of hydrogen. At this point in time, lower bound net section stress for the CGHAZ is not established. Based on the

existing results (*Figure 8*b), it is reasonable to assume that it will be lower than 650 MPa. Experiments will continue to establish lower bound net section stress for CGHAZ.

a)   b)
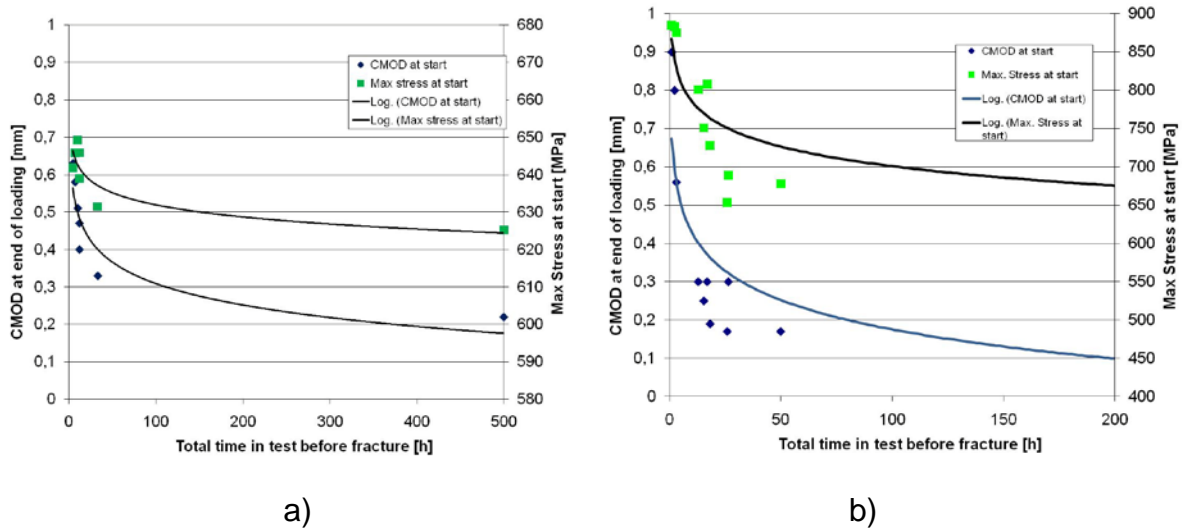
Figure 8 SENT test results. Net section stress and CMOD as a function of time to fracture. a) BM b) CGHAZ

Modelling
Four node bi linear plain strain elements with full integration were used for the stress and cohesive models. In the cohesive analyses, cohesive elements were located at the symmetry axis. 4 node linear mass diffusion elements were applied for the diffusion analyses. Due to symmetry only half the specimens were modelled. Sections of the model representing the CGHAZ specimens are shown in *Figure 9*. The cohesive elements are denoted with black crosses at the symmetry axis of the model (left). Cohesive elements are 15 – 20 μm close to the crack tip, which ensures good resolution of the crack tip stress field.

a)   b)
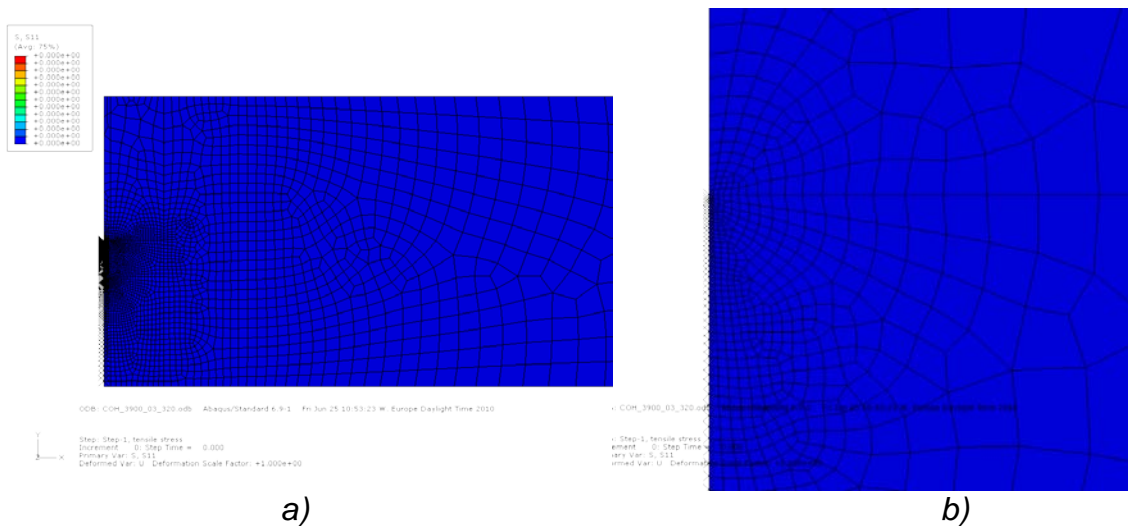
Figure 9 Snapshots of FE model of CGHAZ SENT specimen. a) 3.7 x b) Close up of the notch area.

The models were given the same constant tensile stress as in the SENT testing of hydrogen charged samples. Hydrogen concentration is 1.5 ppm, as measured after hydrogen charging. The same concentration is applied at the surface to represent cathodic potential during testing. Failure criterion in the cohesive analyses is zero stress in the first cohesive element.

Model material
Elastic-plastic
Elastic modulus: BM: 200000 MPa, CGHAZ: 208000 MPa, Poissons rate: 0.3
Material curves: stress strain curves representing tensile test result from tensile testing of the BM and CGHAZ material.

Diffusion
Diffusion coefficients as measured in electrochemical permeation cell and corrected with respect to temperature[14]: BM: 1.94×10^{-5} mm^2/s, CGHAZ: 3.39×10^{-6} mm^2/s, solubility: 0.033 ppm mm $\sqrt{N}$ [15].

Initial cohesive energy, Γ_c, of 300 N/mm and 400 N/mm from the J-r testing (ref Figure 7) was taken as starting points for the iteration process of establishing the cohesive parameters giving the best fit to the experiments. For base metal a cohesive opening and initial maximum stress of $\delta_c = 0.3$ mm and $\sigma_c = 1700$ MPa gave best fit to the results. For CGHAZ, cohesive parameters of $\delta_c = 0.3$ mm and $\sigma_c = 3900$ MPa was chosen under the assumption of a lower bound net section stress of 550 MPa. These cohesive parameters will according to eq. 5 give an initial cohesive energy of 287 N/mm for BM and 658 N/mm for CGHAZ. Plots of experimental and simulated results are presented in *Figure 10*.

a)   b)
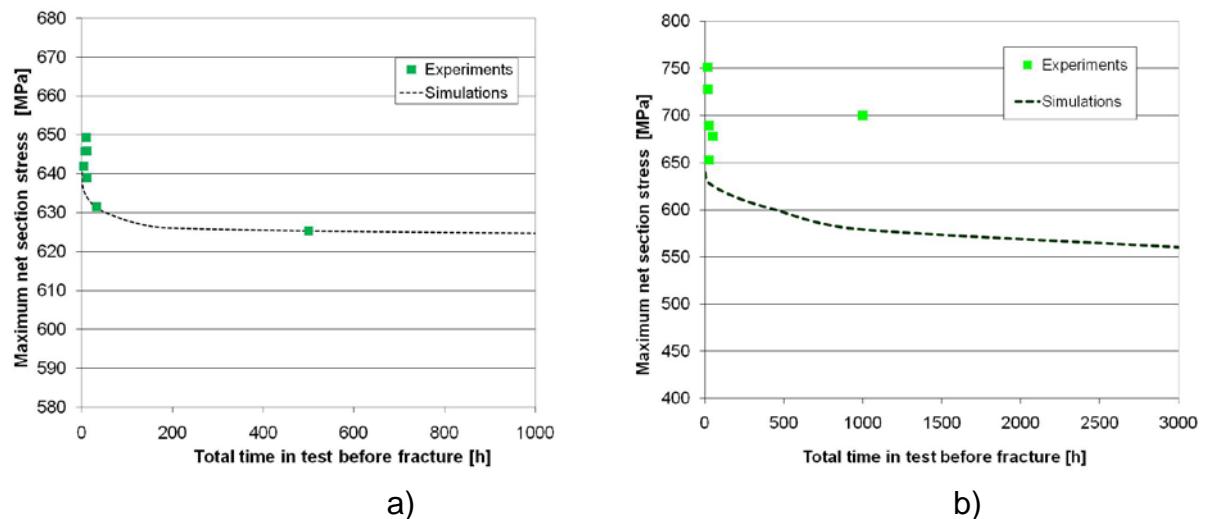
Figure 10 Net section stress at fracture under hydrogen influence - comparison of experiments and simulations a) BM   b) CGHAZ

According to these results base metal, as previously stated, is not very sensitive to hydrogen. Lower bound stress equals 1.29 times the yield strength of the base metal, *Figure 10*a. Assuming a lower bound net section stress of CGHAZ material of 550 MPa, this equals only 68% of the yield strength (809 MPa), which will imply a clear influence of hydrogen, *Figure 10*b. Lower bound net section stresses of 650 MPa and

550 MPa, will according to equation 5 and 6 give threshold stress intensities K_{HE} of 155 and 146 MPa√m. These are reasonably high toughness values. There is however uncertainty related to the CGHAZ results, since the lower bound stress level is still not experimentally verified.

Concept of simulating hydrogen induced fracture in a welded joint
To evaluate the criticality of hydrogen induced fracture in a welded joint one needs, in addition to the material and hydrogen related properties as described, information on residual and applied stress and distribution of hydrogen after welding and cooling. By using imported resulting residual stress fields and hydrogen concentration fields after welding from simulations in WeldSimS[16] as initial conditions in the ABAQUS simulations, such an evaluation is possible. To illustrate the concept a simplified welded joint geometry model is prepared. Since we have established the BM and the CGHAZ properties, but not the WM properties, the concept is illustrated applying CGHAZ properties in all regions of the welded joint in the ABAQUS part of the analysis. A section of the model picturing the welded joint with the imported normal residual stress and hydrogen concentration field is presented in *Figure 11*. Note that the model is axisymmetric, representing a circumferential weld in a pipe. The pipe wall thickness is 12 mm and outer pipe diameter 224 mm. Note that the normal tensile residual stress after welding is highest near the root region of the weld (~500 MPa) and compressive (~560 MPa) in the outer weld/HAZ region, see *Figure 11* a. The resulting hydrogen concentration field is pictured in *Figure 11* b, with a maximum of about 7 ppm in the centre of the weld, assuming 10 ppm hydrogen concentration in the weld bead prior to cooling.

a)   b)
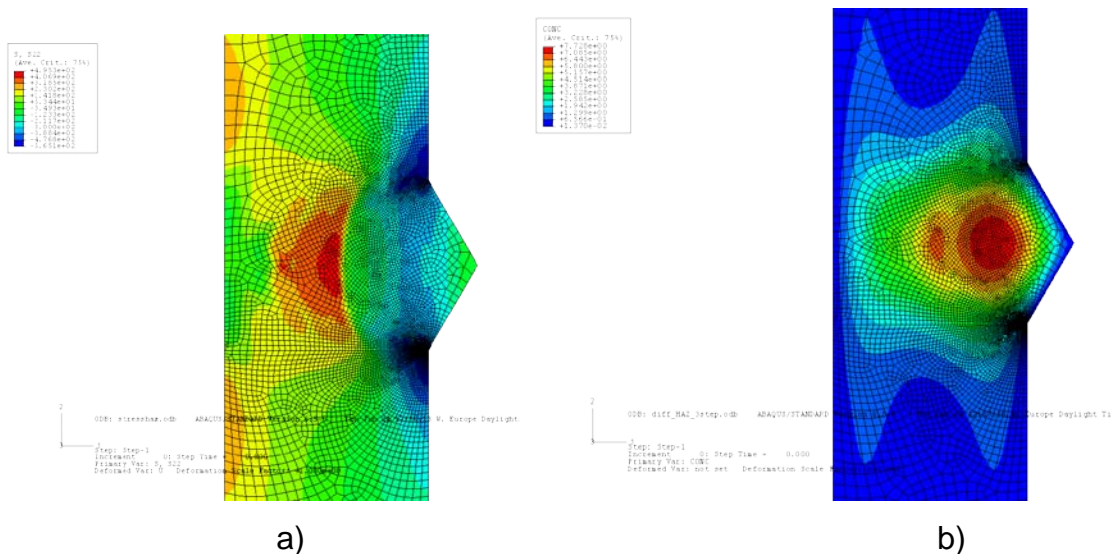
Figure 11 Initial conditions after welding, imported from WeldSimS a) Residual stress b) Hydrogen concentration

The following history was simulated: 1 day of resting in room temperature after welding, followed by seven days with an applied normal tensile stress of 500 MPa. Cohesive elements are located in a cross-sectional predefined path starting from the weld toe (denoted with X's). As shown in *Figure 12*, there is a tensile stress concentration in the weld toe region, but it is not high enough to cause crack initiation

in the cohesive elements. This is mainly due to the residual compressive stress field from welding.
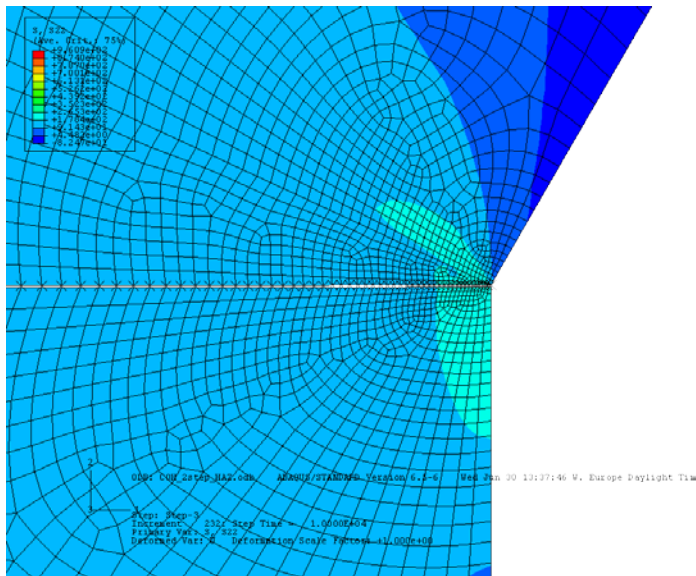
Figure 12 Stress field in weld metal/HAZ region after cohesive simulation. Including influence of residual stress, hydrogen and applied normal tensile stress of 500 MPa for one week.

Discussion

The initial cohesive stresses applied in the simulations are 1700 MPa for BM and 3900 MPa for CGHAZ, which equals $3.5 \cdot \sigma_{p0.2}$ and $4.8 \cdot \sigma_{p0.2}$ respectively. Tvergaard and Huchinson[17] used $4 \cdot \sigma_y$ as the critical cohesive stress in polynomial TSL without hydrogen influence. Later Serebrinsky et al.[9] applied the same critical stress in linear hydrogen influenced TSL's and found good agreement with fracture threshold stresses for high strength steel in aqueous solutions. A value of 3.7 times the yield strengt gave the best fit for cohesive simulation of 25%Cr stainless steel under cathodic protection conditions reported by Olden et. al[13]. The maximum stress applied in the present work is both lower and higher compared to these maximum stress values. The maximum cohesive stress for BM is fairly close to what is reported in literature. The initial cohesive energy for BM is 287N/mm which is close to the estimated cohesive stress of 300 N/mm from SENT testing in air (*Figure 7*a). The maximum cohesive stress for the CGHAZ is as previously mentioned fitted to a limited amount of tests, and more SENT testing at lower stress levels may change the cohesive parameters best fitting the experiments.

Moreover, crack initiation and crack growth measurements during SENT testing submerged in electrolyte have not been performed. This implies that total fracture of the hydrogen charged SENT specimens is represented by a crack initiation (collapse in one element) in the cohesive model. This would further imply that the crack initiation is a critical event. Registered data during constant load testing show that stable crack growth may have taken place prior to the final fracture. As exemplified with a CGHAZ specimen loaded to 0.6 mm CMOD in *Figure 13* a, stable crack growth seem to have grown for about 2 hours prior to the unstable fracture occurring after 3 hours. This is compared to a not fractured specimen from the BM testing, where the CMOD also has increased but later stabilized, see *Figure 13* b. Whether

the deformation is cracking or creep has to be verified by inspection of the fracture surfaces in scanning electron microscope (SEM).
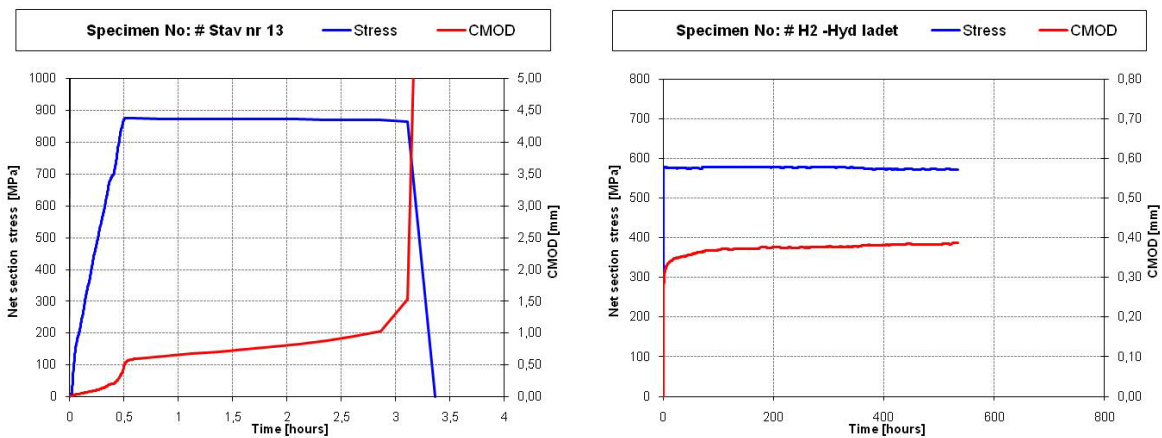
Figure 13 Constant load stress and CMOD curves from SENT testing of hydrogen charged specimens a)CGHAZ, initial CMOD of 0.6 mm and net secton stress of 875 MPa   b) BM, initial CMOD of 0.35 mm and 570 MPa, not fractured.

If initial cracking has taken place prior to final fracture, and the simulations were to be fitted to the time for crack initiation to occur, this would lower the initial cohesive stress.

The presented welded joint simulation must be regarded as an example of how this model can be applied. For conclusions to be drawn regarding stress states, hydrogen distribution and pipe integrity more information is needed. However, there is an indication that residual pressure stresses at the weld toe after welding will improve the resistance towards hydrogen embrittlement in the same region.

Conclusions

Fracture mechanics SENT testing and FE modelling have been performed to establish hydrogen influenced cohesive parameters for X70 structural steel. The following conclusions can be made:

- The tested base metal X70 steel did not fail at net section stresses lower than 1.29 times the 0.2% yield strength and hence, reveals low sensitivity to hydrogen embrittlement.
- Weld simulated coarse grained heat affected zone is prone to fracture at stresses above 70% of the yield strength, which indicates hydrogen embrittlement susceptibility.
- A polynomial traction separation law with intrinsic hydrogen dependant energy works well for the cohesive simulations.
- Cohesive parameters best fitting the experiments for base metal are δ_c=0.3 mm and σ_c=1700 MPa (3.5·σ_y)
- Cohesive parameters applied for CGHAZ are δ_c=0.3mm and σ_c=3900 MPa (4.8·σ_y).
- An example is given proving that the model, given the correct input, can be applied in evaluating the fracture integrity of a welded joint.

13

Further work

For the model to able to predict the structural integrity of a real hyperbaric weld there are several aspects that needs to be addressed. First of all the weld geometry have to be established. This is work on going. Second the model needs material, diffusion and cohesive properties representing all regions, BM, CGHAZ and weld metal. Weld metal testing will be performed as soon as a satisfactory weld procedure is established. More information regarding the hydrogen level of the weld immediately after welding is also required, and will be retrieved by measuring hydrogen pick up during welding (ISO – 3690, 1977-E).

Fracture surface topography of selected hydrogen charged SENT testing will be performed in SEM to clarify the length of eventual hydrogen induced cracking. Finally the model will be developed to handle 3D simulations, which includes the development of 3D hydrogen informed cohesive elements.

References

[1]   ABAQUS, Version 6.5, and 6.9 Users' manual, ABAQUS Inc. **2004** and **2009**.

[2]   V. Olden, C. Thaulow, R. Johnsen, E. Østby, T. Berstad, Engineering Fracture Mechanics, **2008**, 75 (8).

[3]   P. Sofronis, R.M. McMeeking, Journal of the Mechanics and Physics of Solids, **1989**, 37 (3).

[4]   A.H.M. Krom, R.W.J. Koers, A. Bakker, Journal of the Mechanics and Physics of Solids, **1999**, 47.

[5]   R.A. Oriani, Acta Metall., **1970**, 18.

[6]   A. Taha, P. Sofronis, Engineering Fracture Mechanics, **2001**, 68.

[7]   A. Needleman, A., Journal of Applied Mechanics, **1987**, 54.

[8]   V. Tvergaard, Materals Science and Engineering A, **1990**, 125 (2).

[9]   S. Serebrinsky, E.A. Carter, M. Ortiz, Journal of the Mechanics and Physics of Solids, **2004**, 52.

[10]   D.E. Jiang , E.A. Carter, Acta Materialia, **2004**, 52.

[11]   E. D. Hondros, M. P. Seah, Metallurgical Transactions A, **1977**, 8A.

[12]   I. Scheider, W. Brocks, Engineering Fracture Mechanics, **2003**, 70.

[13]   V. Olden, C. Thaulow, R. Johnsen, E. Østby, T. Berstad. Engineering Fracture Mechanics, **2009**, 76.

[14]   M. Skjellerudsveen, O.M. Akselsen, V. Olden, R. Johnsen and A. Smirnova, To be published at EuroCorr 2010, Moscow 13.-17. September, **2010**

[15]   ABAQUS, Version 6.3, Example problems manual, Hibbitt, Karlsson & Sorensen Inc., **2000**, p. 6.1.2-1

[16]   H. G. Fjær, J. Liu, M. M'Hamdi and D. Lindholm, in Mathematical Modelling of Weld Phenomena, **2007**, 8.

[17]   V. Tvergaard, J.W. Hutchinson, Journal of Mechanics Physics and Solids, **1992**, 40 (6)